Supporting Information

for

MALDI-2 for the enhanced analysis of N-linked glycans by mass spectrometry imaging

Bram Heijs[1,2,*], Alexander Potthoff[1], Jens Soltwisch[1,3], Klaus Dreisewerd[1,3]

[1] Institute of Hygiene, University of Münster, Robert-Koch-Str. 41, 48149 Münster, Germany.

[2] Center for Proteomics and Metabolomics, Leiden University Medical Center, Albinusdreef 2, 2333 ZA Leiden, The Netherlands.

[3] Interdisciplinary Center for Clinical Research (IZKF), University of Münster, Domagkstr. 3, 48149 Münster, Germany.

* Corresponding author: b.p.a.m.heijs@lumc.nl

Table of Content:

Supplementary Methods

timsTOF flex MALDI-2 modifications – As previously described by Soltwisch *et al.* [34], the instrument has been equipped with a Q-switched, frequency quadrupled Nd:YAG (wavelength 266 nm) NL 204-1k-FH laser (Ekspla, Vilnius, Lithuania) with a 1 kHz repetition rate, and 7 ns pulse duration. The PI laser is shaped by a beam expander (1:3, CaF_2 lenses), and focused using a CaF_2 lens (f = 60 mm). The beam has a focal diameter of approximately 85 µm, and is located 500 µm in front of the ablation position. The PI laser is guided through the source into a beam dump, via two CaF_2 windows located on the top and bottom of the source. The interlaser delay is realized by synchronizing the lasers using the Q-switch trigger signal of the SmartBeam 3D laser and an electronic pulse delay unit (Quantum Composer 9214; Schulz Electronic, Baden-Baden, Germany).

Oligosaccharide Standard Preparation – To assess the potential benefits of MALDI-2 for the detection of oligosaccharides, maltoheptaose (0.5 mM) was premixed with 41 mM of NOR MALDI matrix in 50:50 (% v/v) EtOH:dH_2O, and homogeneously sprayed (167 pmol mm^{-2}) on a Superfrost microscope glass slide (Thermo Scientific) using a SimCoat spray-robot (Sono-Tek, Milton, NY) with ultrasonic AccuMist nozzle (Sono-Tek). Additionally, a maltoheptaose dilution series was prepared using the same protocol (Supplementary Table S-1). Standard *N*-glycans (H4N4, H4N4F1, and H5N4F1) were dissolved in dH_2O at 10 pmol μL^{-1}, pre-mixed 1:1 with NOR (41 mM in EtOH), and analyzed after spotting 1 μL on a SCOUT-384 MALDI target plate with ground steel surface (Bruker Daltonics).

Supplementary Table S-1. Maltoheptaose dilution series used to determine limits of detection in the positive and negative ion mode MALDI-2 experiments

Maltoheptaose concentration in solution	**Maltoheptaose amount sprayed on target**	**Maltoheptaose per scanned pixel (1280 µm²)**
(mol L^{-1})	*(mol mm^{-2})*	*(amol)*
5.0 x10^{-5}	1.67 x10^{-11}	22 x10^{3}
5.0 x10^{-6}	1.67 x10^{-12}	2 x10^{3}
5.0 x10^{-7}	1.67 x10^{-13}	215
5.0 x10^{-8}	1.67 x10^{-14}	22
5.0 x10^{-9}	1.67 x10^{-15}	2

MALDI-2 Parameter Optimization – Experiments for MALDI-2 parameter optimization were conducted on a Synapt G2-S HDMS mass spectrometer (Waters/Micromass, Manchester, U.K.), modified as described in Kettling *et al.* [ESI-1], and Soltwisch *et al.* [22]. Data acquisition and processing were performed as described in Potthoff *et al.* [25]. Briefly, a setup combining hardware components and LabVIEW-based (National Instruments, Austin, TX) software allowed to automatically change, monitor and optimize the following key input parameters: i) ablation laser pulse energy, ii) PI laser energy, iii) cooling gas pressure (p), and iv) interlaser pulse delay (τ). Pseudo-2D ion images were recorded at a pixel diameter of 60 μm^2 in a mass range of *m/z* 50-2000 using the standard workflow of the HDimaging and Mass Lynx softwares (Waters). During the experiments, two input parameters were changed systematically (one constant parameter set was recorded for 10 pixels with 20 laser shots per pixel). Laser energies were varied between 0 and 25 μJ for the ablation laser, and between 0

and 230 μJ for the PI laser. The cooling gas pressure, p, was varied between 0.5 and 3.3 mbar, and the interlaser delay, τ, was varied between 0 and 60 μs.

Following data acquisition, a lock mass correction, performed with the known masses of maltoheptaose (positive ion mode m/z_{calcd} 1175.370 $[C_{42}H_{72}O_{36} + Na]^+$, and negative ion mode m/z_{calcd} 1151.373 $[C_{42}H_{72}O_{36} - H]^-$), was applied and the data was then converted to centroid spectra with the "Accurate Mass Measure" tool of the MassLynx software. Recalibrated MS data were converted to mzML format using ProteoWizard [ESI-2] software and were then converted to imzML [ESI-3] using an imzML converter developed by Race *et al*. [ESI-4]. With an in-house developed Python script, utilizing the pyimzML package [ESI-5], the detector readouts and experiment-parameter settings were post-processed and combined with the spectral data. Plots of the experimental data were either created using Python or OriginPro 2020 (OriginLab, Northampton, MA).

Supplementary References

If reference was mentioned in manuscript, manuscript numbering has been applied.

[ESI-1] Kettling, H.; Vens-Cappell, S.; Soltwisch, J.; Pirkl, A.; Haier, J.; Muthing, J.; Dreisewerd, K. MALDI mass spectrometry imaging of bioactive lipids in mouse brain with a Synapt G2-S mass spectrometer operated at elevated pressure: improving the analytical sensitivity and the lateral resolution to ten micrometers. *Anal. Chem.* **2014**, *86*, 7798–7805.

[ESI-2] Chambers, M. C.; Maclean, B.; Burke, R.; Amodei, D.; Ruderman, D. L.; Neumann, S.; Gatto, L.; Fischer, B.; Pratt, B.; Egertson, J.; Hoff, K.; Kessner, D.; Tasman, N.; Schulman, N.; Frewen, B.; Baker, T.A.; Brusniak, M.-Y.; Paulse, C.; Creasy, D.; Flashner, L.; Kani, K.; Moulding, C.; Seymour, S.L.; Nuwaysir, L.M.; Lefebvre, B.; Kuhlmann, F.; Roark, J.; Rainer, P.; Suckau, D.; Hemenway, T.; Huhmer, A.; Langridge, J.; Connolly, B.; Chadick, T.; Holy, K.; Eckels, J.; Deutsch, E.W.; Moritz, R.L.; Katz, J.E.; Agus, D.B.; MacCoss, M.; Tabb, D.L.; Mallick, P. A cross-platform toolkit for mass spectrometry and proteomics. *Nat. Biotechnol.* **2012**, *30*, 918–920.

[ESI-3] Schramm, T.; Hester, Z.; Klinkert, I.; Both, J.-P.; Heeren, R. M. A.; Brunelle, A.; Laprevote, O.; Desbenoit, N.; Robbe, M.-F.; Stoeckli, M.; Spengler, B.; Roempp, A. imzML--a common data format for the flexible exchange and processing of mass spectrometry imaging data. *J. Proteomics* **2012**, *75*, 5106–5110.

[ESI-4] Race, A. M.; Styles, I. B.; Bunch, J. Inclusive sharing of mass spectrometry imaging data requires a converter for all. *J. Proteomics* **2012**, *75*, 5111–5112.

[ESI-5] alexandrovteam. pyimzML. https://github.com/alexandrovteam/pyimzML (accessed February 12, 2020).

[22] Soltwisch, J.; Kettling, H.; Vens-Cappell, S.; Wiegelmann, M.; Muthing, J.; Dreisewerd, K. Mass spectrometry imaging with laser-induced postionization. *Science* **2015**, *348*, 211–215.

[25] Potthoff, A., Dreisewerd, K., Soltwisch, J. Detailed characterization of the post-ionization efficiencies in MALDI-2 as a function of relevant input parameters. *J. Am. Soc. Mass Spectrom.* **2020**, *Under revision*.

[29] Soltwisch, J.; Heijs, B.; Koch, A.; Vens-Cappell, S.; Höhndorf, J.; Dreisewerd, K. MALDI-2 on a trapped ion mobility quadrupole time-of-flight instrument for rapid mass spectrometry imaging and ion mobility separation of complex lipid profiles. *Anal. Chem.* **2020**, *Article ASAP*.

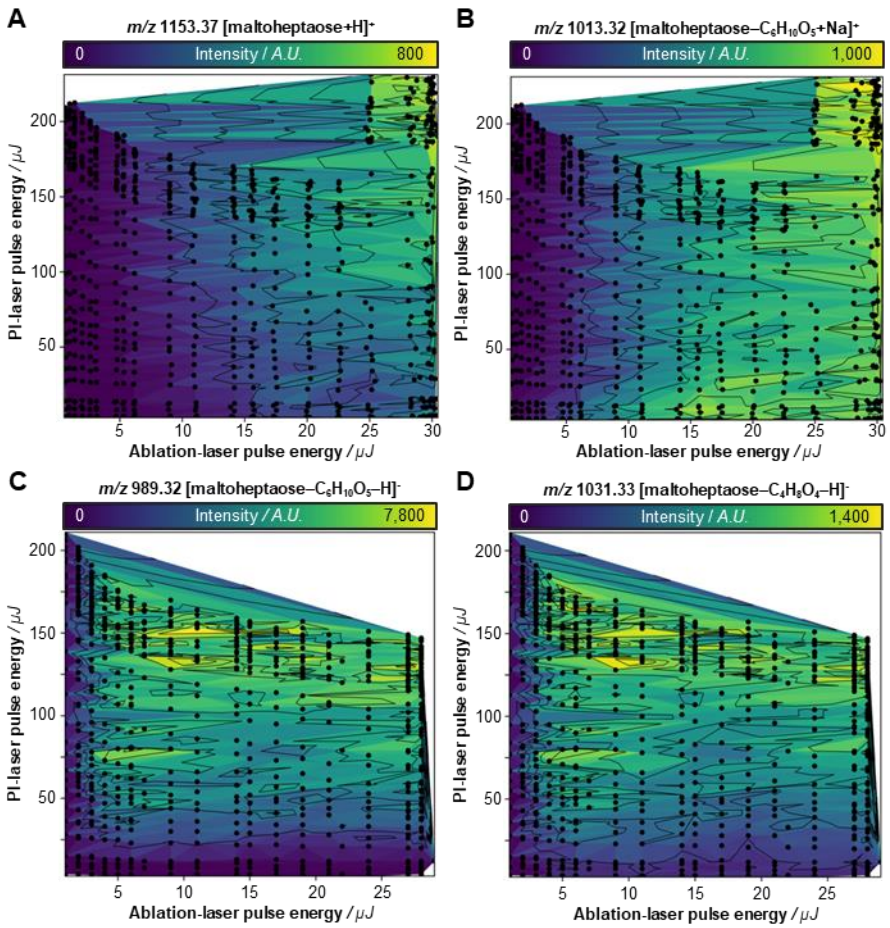

Supplementary Figure S-1: The effect of laser pulse energies on the fragmentation of oligosaccharides. (A) The effect of ablation laser pulse energy and post-ionization laser pulse energy on the signal intensity of the protonated maltoheptaose ion (*m/z* 1,153.37 [maltoheptaose + H]$^+$). The experiment, varying both laser pulse energies, was performed at a fixed cooling gas pressure of 2.0 mbar, and an inter-laser delay of 10 µs. Black dots represent the individual measurements (average of n = 10 pixels). The highest signal intensities were observed when high ablation and post-ionization laser energies were applied. However, severe fragmentation occurred under these conditions, resulting in **(B)** hexose losses (*m/z* 1,013.32 [maltoheptaose – $C_6H_{10}O_5$ + Na]$^+$) and cross-ring-fragmentation (not shown). Fragmentation also occurred in negative ion-mode. Increases in intensity of the loss of hexose **(C)** and cross-ring fragmentation **(D)** peaks occurred under similar conditions when the deprotonated maltoheptaose signal was boosted.

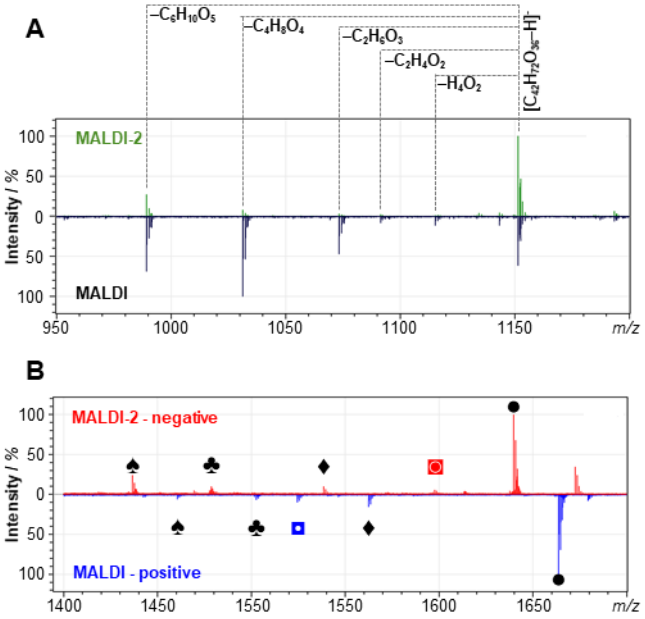

Supplementary Figure S-2: The effect of laser-induced post-ionization MALDI-MS on the analysis of oligosaccharides. (A) Negative ion-mode MALDI-2-MS (*top, green*), and MALDI-MS (*bottom, black*) example spectra of maltoheptaose DP7 (*m/z* 1,151.37 $[C_{42}H_{72}O_{36} – H]^-$). The instability of deprotonated oligosaccharide ions is reflected by the maltoheptaose fragmentation, occurring under both MALDI, and MALDI-2 conditions. The signal intensity of the deprotonated maltoheptaose signal was boosted substantially by the MALDI-2 process (3.0 mbar cooling gas pressure, 30 µs inter-laser delay, 250 µJ PI laser energy, 0.34 µJ ablation laser energy). The absolute intensity of the fragment ions increased as well, but much less compared to the „parent ion“. Due to the presence of structural isomers among the fragment ions, fragments are shown as the net change to the molecular formula of maltoheptaose. **(B)** Negative ion-mode MALDI-2-MS (*top, red*), and positive ion-mode MALDI-MS (*bottom, blue*) of biantennary complex-type *N*-glycan H5N4 (where H = hexose, and N = *N*-acetylhexosamine; symbol: ●**;** negative ion-mode: *m/z* 1,639.58 $[C_{62}H_{104}N_4O_{46} – H]^-$; positive ion-mode: *m/z* 1,663.58 $[C_{62}H_{104}N_4O_{46} + Na]^+$). Fragmentation of H5N4 occurred in both polarities under the described conditions. Fragment ions occurring in both negative and positive ion-mode have been highlighted with equal symbols (♠: $–C_8H_{13}N_1O_5$, ♣: $–C_8H_8O_5$, ♦: $–C_4H_7NO_2$), unique fragments for either polarity are indicated with unique symbols (◘: *unknown*, ◙: $–C_2H_2O$).

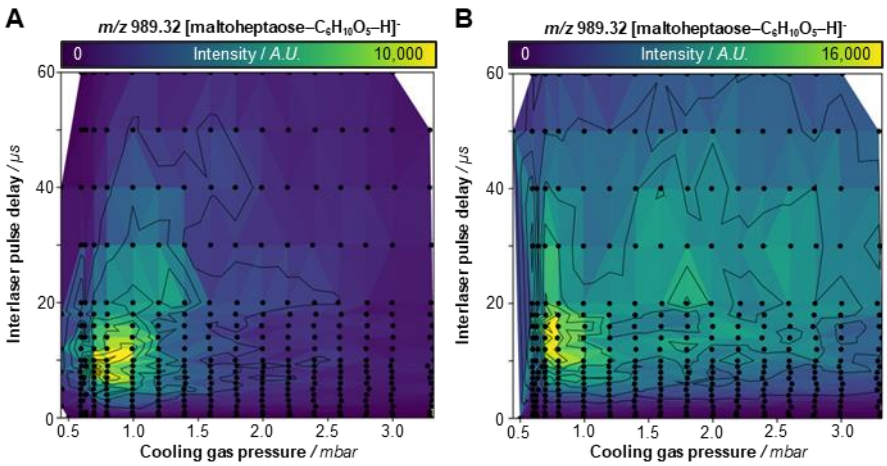

Figure S-3: Fragmentation at varying cooling gas pressure and inter-laser delay. Maltoheptaose fragmentation (minus hexose) as a function of cooling gas pressure, and inter-laser delay. Data was recorded with low **(A)** and high **(B)** ablation laser energies. It becomes apparent that most fragmentation occurs at low pressure, and short inter-laser pulse delay.

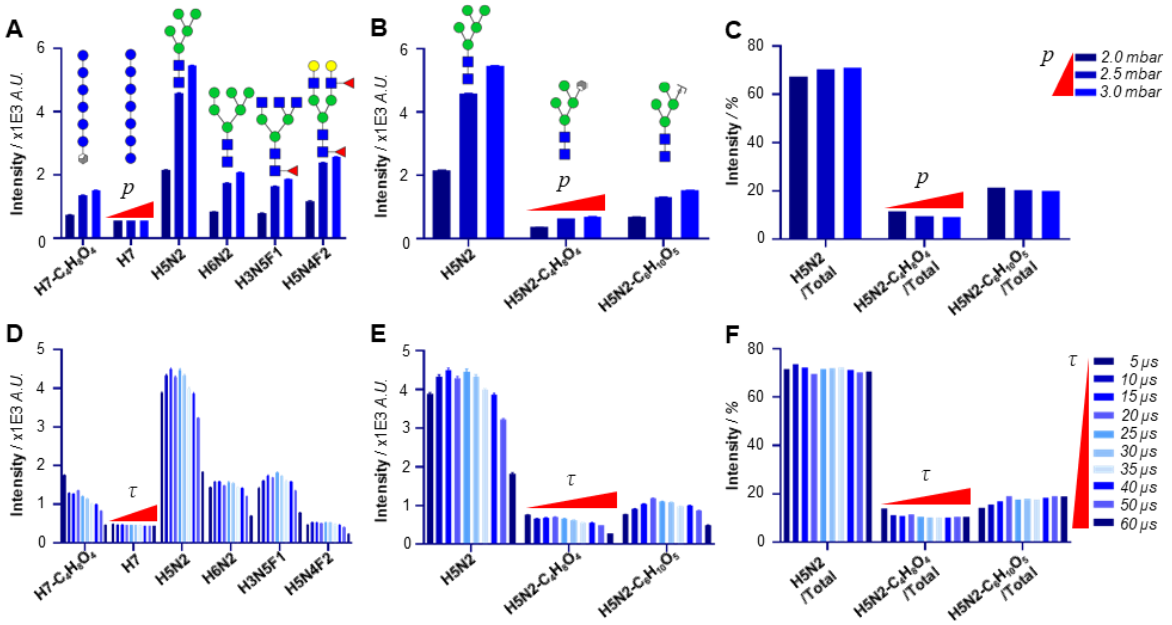

Figure S-4: The effects of cooling gas pressure, and inter-laser delay on negative ion-mode MALDI-2-MSI of *N*-glycans in human cerebellum. (A) Average intensities of various *N*-glycans (H5N2, H6N2, H3N5F1, and H5N4F2), maltoheptaose (H7), and maltoheptaose fragment (H7 – $C_4H_8O_4$) after MALDI-2-MSI at varying cooling gas pressure. Structures represent the sugar composition, but may have isomeric species. Data was recorded with a 30 µs inter-laser delay. Absolute intensities were normalized to the maltoheptaose internal standard. **(B)** Absolute intensities for H5N2, and two H5N2 fragments (– $C_4H_8O_4$, and – $C_6H_{10}O_5$) after MALDI-2-MSI of *N*-glycans at varying cooling gas pressure. **(C)** Relative formation of H5N2, and two H5N2 fragments (– $C_4H_8O_4$, and – $C_6H_{10}O_5$) at varying cooling gas pressure. **(D)** Average intensities of various *N*-glycans (H5N2, H6N2, H3N5F1, and H5N4F2), maltoheptaose (H7), and maltoheptaose fragment (H7 – $C_4H_8O_4$) after MALDI-2-MSI at varying inter-laser delay. Data was recorded at a 2.5 mbar cooling gas pressure. Absolute intensities are normalized to the maltoheptaose internal standard. **(E)** Absolute intensities for H5N2, and two H5N2 fragments (– $C_4H_8O_4$, and – $C_6H_{10}O_5$) after MALDI-2-MSI of *N*-glycans at varying inter-laser delay. **(F)** Relative formation of H5N2, and two H5N2 fragments (– $C_4H_8O_4$, and – $C_6H_{10}O_5$) at varying inter-laser delay.

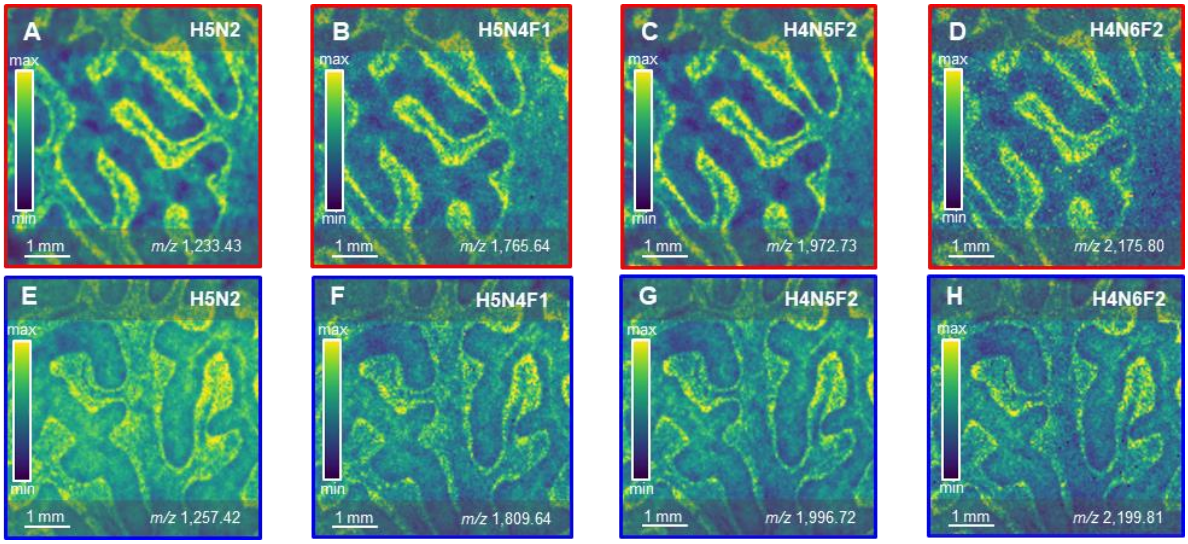

Figure S-5: Example images of various N-glycan species in the human cerebellum. (A-D) In red squares the images obtained using negative ion mode MALDI-2-MSI, and **(E-H)** in blue squares the images obtained for the same glycan species in positive ion mode MALDI-MSI of the human cerebellum.

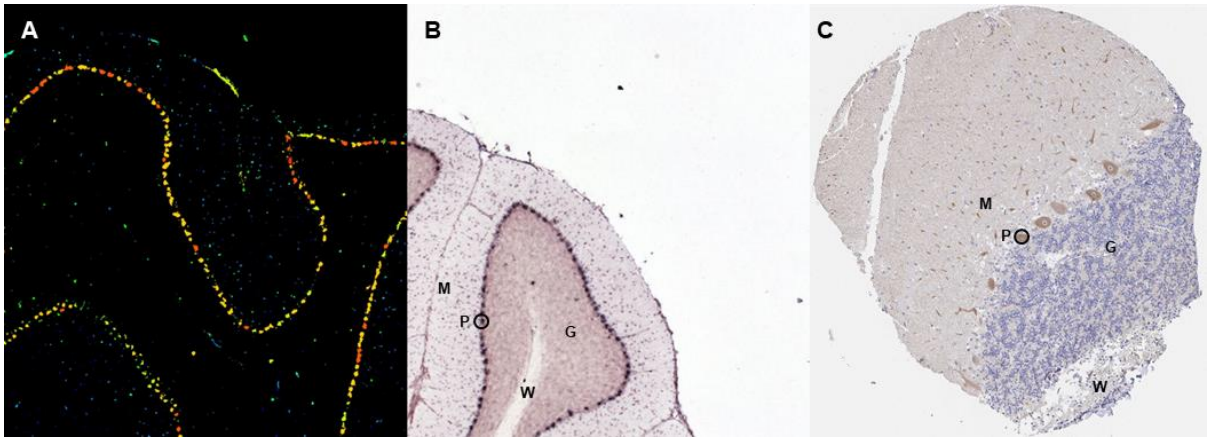

Figure S-6: Supplementary Figure S5: Man1a1 expression in human brain and mouse brain. The expression of the mannosidase 1, alpha (man1a1) enzyme in mouse brain (A, expression profiling; B, in-situ hybridization) and human (54 y/o male) brain (C, immunohistochemistry) obtained from the Allen Mouse Brain atlas (http://www.brain-map.org) and the Human Protein Atlas (http://www.proteinatlas.org) respectively. Man1a1 expression occurs predominantly in the Purkinje cell layer (P) and the granular layer (G) of the brain, in comparison to the white matter (W) and molecular layer (M). Man1a1 is one of the enzymes of the *N*-glycan biosynthesis pathway. The enzyme is responsible for trimming a mannose residue from the H9N2 glycan, to produce H8N2 in the endoplasmatic reticulum (ER).